Chemical Dealloying Synthesis of CuS Nanowire-on-Nanoplate Network as Anode Materials for Li-Ion Batteries

Zhifeng Wang [1] [iD], **Xiaomin Zhang** [1], **Yongguang Zhang** [1,*], **Man Li** [1], **Chunling Qin** [1,*] [iD] and **Zhumabay Bakenov** [2] [iD]

[1] School of Materials Science and Engineering, Hebei University of Technology, Tianjin 300130, China; zfwangmail@163.com (Z.W.); xmZhang1223@163.com (X.Z.); mlimail2017@163.com (M.L.)

[2] Synergy Innovation Institute of GDUT, Heyuan 517000, China; zbakenov@nu.edu.kz

[*] Correspondence: yongguangzhang@hebut.edu.cn (Y.Z.); clqin@hebut.edu.cn (C.Q.);
Tel.: +86-22-6020-1447 (Y.Z.); +86-22-6020-4477 (C.Q.)

Abstract: CuS is a metal sulfide anode material used in constructing lithium ion batteries (LIBs) with great promise. However, its practical application is limited by rapid capacity decline, poor cycling, and rate performance. In this work, the CuS nanowire-on-nanoplate network is synthesized through an improved dealloying method under two contrasting reaction temperatures. When used as an LIB anode, the as-obtained CuS network exhibits superior cycling performance (420 mAh·g^{-1} retained after 100 cycles at 0.2 C). When at 3 C, it still delivers a capacity of around 350 mAh·g^{-1}. The improved electrochemical performances of the CuS anode should be attributed to the well-designed nanowire-on-nanoplate network structure in which the introduction of nanowires improves Li storage sites, shortens Li-ion diffusion distance, enhances the conductivity of active materials, and offers multiscale spaces for buffering the volume variation. The fabrication route adopted in this paper has an important significance for developing the dealloying technique and designing more suitable anode structures for LIBs.

Keywords: dealloying; CuS; anode; Li-ion battery; metallic glass

1. Introduction

With the fast development of electronic devices, lithium ion batteries (LIBs) that adopt commercial graphite anodes have not satisfied the increasing demand for large capacity and high energy density because the capacity of graphite is only 372 mAh·g^{-1} [1,2]. Therefore, investigating larger specific capacity alternative anode materials has brought great interest [3,4]. Currently, metal sulfides as new generation anode materials are studied widely because of their higher theoretical capacities. Due to the excellent electrical conductivity (~10^{-3} S·cm^{-1}), abundant resource, and large theoretical capacity (560 mAh·g^{-1}) [5,6], CuS can be utilized as an electrode material for LIBs.

Despite many advantages, the practical application of CuS is hindered by rapid capacity decay, which is caused by the huge volume change and active material loss due to formation and dissolution of intermediate products. This includes polysulfides Li$_2$S$_x$ ($2 < x < 8$) during repeating charge/discharge processes [7]. To solve these problems, many efforts including nanostructuring and hybridizing CuS with carbon have been performed. These measures can prevent the aggregation and pulverization of the electrodes, enhance electrical conductivity, and further improve their electrochemical performances. Among different attempts, nanostructuring is one of the most simple and effective routes. Nanostructured CuS with various morphologies [7–9] including nanospheres, nanowires and nanoflakes have been fabricated. These nanostructures, with small particle sizes

and plenty of space, are able to decrease the internal stress and alleviate the volume change upon cycling [10].

Up to now, a variety of methods such as the sol-gel technique [11], the template method [12], the thin film deposition method [13], and solvothermal synthesis [14] have been successfully applied to fabricate nanostructured CuS. However, the disadvantages of these techniques such as prolonged processing, a complicated preparation approach, and a low yield result in higher production cost of CuS anodes. As such, a simple and low cost route for preparing nanostructured CuS materials is urgently needed.

Dealloying as an ancient and popular technique to fabricate nanoporous metals [15,16] has been recently extended into a new method for synthesizing nanostructured metal oxides/sulfides [17–19] with different morphologies. Morphology controllable CuS nanoplates were successfully acquired by Zhu et al. [19,20] through the simple and low-cost dealloying method. However, these nanoplates showed poor cycling abilities when they were directly used as the anodes of LIBs. This may be due to the low connectivity and the large nanoplate size. In this paper, we report a simple and improved dealloying method to enhance the connectivity by generating nanowires among and on different nanoplates. CuS nanowire-on-nanoplate networks were successfully fabricated via a two-step chemical dealloying route under two contrasting reaction temperatures. In this situation, superficial nanostructures and Li storage sites were dramatically increased and the conductivity of anode materials was enhanced. As a result, an improved electrochemical performance was obtained. The fabrication route adopted in this paper has important significance for developing a dealloying technique and designing more suitable anode structures for LIBs.

2. Materials and Methods

2.1. Preparation of Materials

$Ti_{40}Cu_{60}$ ingot was first obtained by arc melting of Ti and Cu metals (99.99 wt. %, purchased from China New Metal Materials Technology Co., Ltd., Beijing, China). Then the $Ti_{40}Cu_{60}$ metallic glass ribbons with 20~25 μm in thickness and 1.2~1.5 mm in width as the dealloying precursors were prepared by a previously reported melt-spinning method [21,22]. The glassy ribbons were cut into 2 cm in length. CuS nanostructures were then synthesized by the chemical dealloying of the glassy ribbons in 15 M H_2SO_4 solutions. During the dealloying process, Ti elements were selected and dissolved into electrolytes. Cu elements left behind were sulfurated by the sulphur atom in highly concentrated H_2SO_4 solutions and further self-assembled into CuS nanostructures. The dealloying was performed in an YT-r100 reaction kettle (Yantu Experimental Equipment Co., Ltd., Tianjin, China) at two contrasting reaction temperatures. The first reaction was performed at 90 °C for 60 h to form the CuS nanoplate matrix. Generally, a reaction at high temperature brings about a product with a big size. To prepare nanowires with a small size, a secondary dealloying reaction was carried out at 10 °C for 36 h. The synthesis process of the CuS sample is represented in Figure 1. It is worth noting that the dealloying strategy adopted in this paper shows some differences to the previous dealloying processes, which reflects in two contrasting reaction temperatures. For a temperature-sensitive chemical reaction, it may bring us two kinds of reaction products either in morphology or in composition. CuS nanowires, which were usually produced from complex reaction conditions, were also obtained by dealloying at a low temperature process in this research study. That opens a door for us to design and fabricate dealloying products in various shapes and create more interesting composite structures. The CuS nanowire-on-nanoplate networks were finally obtained after being washed in ethyl alcohol, centrifuged two times, and then dried under vacuum at 60 °C for 12 h. By dealloying $Ti_{40}Cu_{60}$ glassy ribbons in 15 M H_2SO_4 solutions for 60 h at 90 °C, the CuS nanoplates were also prepared for a comparison.
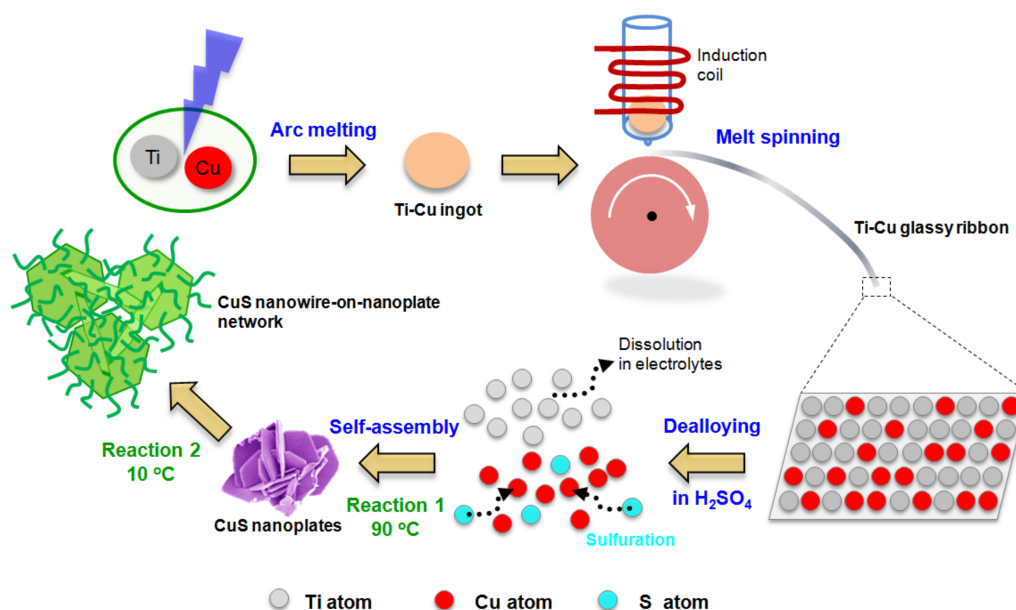
Figure 1. Schematic showing the synthesis process of the CuS nanowire-on-nanoplate network.

2.2. Materials Characterization

The phase analysis of the dealloying products was performed on an X-ray diffraction (XRD, D8 Advance, Bruker, Karlsruhe, Germany) system alongside Cu Kα radiation. The valence state of the samples was characterized using X-ray photoelectron spectroscopy (XPS, Thermo Fisher Scientific, Waltham, MA, USA). The morphology of the products was observed by a scanning electron microscope (SEM, Nova nanoSEM 450, FEI, Hillsboro, OR, USA) equipped with energy dispersive X-ray spectroscopy (EDS, Oxford Instruments, Oxford, Oxfordshire, United Kingdom) and a high-resolution transmission electron microscope (TEM, JEM-2010F, JEOL, Tokyo, Japan).

2.3. Electrochemical Measurements

For testing the electrochemical performance, CuS powders (70 wt. %), Super-P (10 wt. %, TIMCAL, CAS number: 1333-86-4), and carboxymethyl cellulose (20 wt. %, Aladdin, CAS number: 9004-32-4) were mixed in ultra-pure water (18.2 MΩ cm) and grinded in an agate mortar manually for 30 min to make a slurry, which was bladed on a Cu foil and dried at 70 °C for 12 h. The average mass loading of the active material was calculated to be 1.0~1.1 mg·cm^{-2} through the mass difference of Cu disks with and without electrode materials. Half-cells (CR2032 coin cells) were assembled in a glove box filled with argon. The Li plate was used as the counter electrode. The electrolyte is a solution of 1 mol·L^{-1} LiPF$_6$ (Aladdin, CAS number: 21324-40-3) in ethylene carbonate (EC, Aladdin, CAS number: 96-49-1) and dimethyl carbonate (DMC, CAS number: 616-38-6) with the volume ratio of 1:1. A Celgard 2400 porous membrane was used as the separator. The Galvanostatic charge and discharge measurements were recorded by using a CT-4008 battery cycler system (Xinwei, Shenzhen, China) within a voltage range between 1.0 V to 3.0 V (vs. Li$^+$/Li). Cyclic voltammetry (CV) measurements were conducted using an Im6e electrochemical testing system (Zahner, Kronach, Germany) in a potential range between 1.0 V to 3.0 V (vs. Li$^+$/Li) at a scanning rate of 0.1 mV·s^{-1}. The frequency of electrochemical impedance spectroscopy (EIS) measurements ranged from 10 mHz to 100 kHz.

3. Results and Discussion

Figure 2a presents the SEM image of the glassy ribbon after dealloying. It can be seen that the sample is macroscopically stacked by nanoplates, which form an interconnected network. The thickness of the nanoplates is about 25 nm to 40 nm. The CuS nanoplates distribute uniformly and show porous

feature, which is favorable for the conduction of electrical carriers. Figure 2b is an EDS analysis of the sample. It is found that the sample mainly contains the elements of Cu and S. The absence of Ti confirms that Ti is completely removed from the alloy during the process of dealloying in the sulfuric acid solution. The presence of a small amount of carbon and oxygen may be due to the superficial carbon deposition and oxygen absorption of samples in the washing, drying, storage, and even testing process.
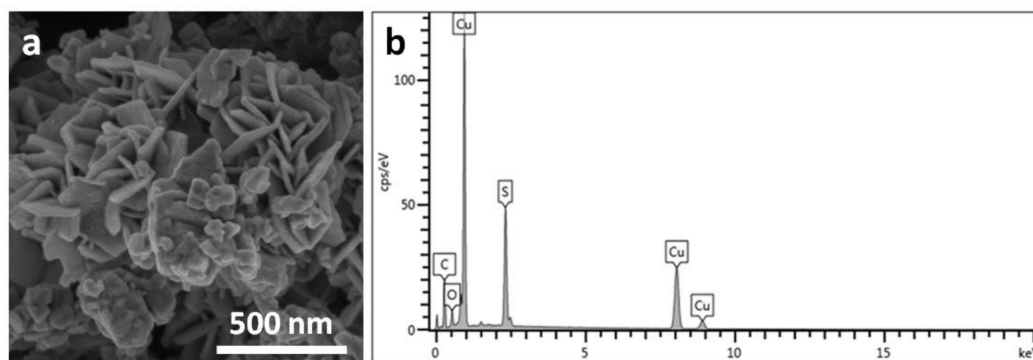

Figure 2. Scanning electron microscope (SEM) image (**a**) and corresponding energy-dispersive X-ray spectroscopy (EDS) analysis (**b**) of the sample after dealloying.

A clear nanowire-on-nanoplate structure is uncovered by TEM in Figure 3a,b. The nanowires with 4 nm to 7 nm in width and 40 nm to 60 nm in length were uniformly dispersed on the surface of the nanoplate matrix. This structure presents a clear difference in a superficial feature compared with previously reported CuS nanoplates. The generation of nanowires strongly improves the connectivity of neighboring nanoplates and the specific surface area as well. The crystallinity of the sample is satisfactory and the lattice fringes of CuS can be observed in Figure 3c. The lattice spacing of 0.189 nm corresponds to the (110) crystal face of CuS. Figure 3d presents the selected area of the electron diffraction (SAED) pattern. The radius of the polycrystalline diffraction pattern is 0.156 nm, 0.189 nm, and 0.281 nm, which corresponds to the (116), (110), and (103) crystal faces of CuS, respectively.

Figure 4a shows the XRD pattern of the original $Ti_{40}Cu_{60}$ sample. It demonstrates a pure homogeneous amorphous structure due to the characteristic of a broad peak without appreciable crystal peaks. Figure 4b is the XRD spectrum of the sample after dealloying. The obvious CuS diffraction peaks of (100), (101), (102), (103), (006), (105), (106), (008), (110), (108), (116), and other crystal faces are detected. These diffraction peaks coincide with the JCPDS Card No. 06-0464, which indicates that CuS with high crystallinity was obtained after dealloying. Further information was obtained from the XRD pattern and the JCPDS Card. It indicates that the as-obtained CuS possesses a hexagonal system structure in which the space group is P63/mm. The lattice constant *a* equals 0.3792 nm and *c* equals 1.6344 nm. The Cu 2p and S 2p core levels XPS spectra for the CuS nanowire-on-nanoplate network are displayed in Figures 4c and 4d. Figure 4c is the Cu 2p spectrum in which 933.1 eV and 953.3 eV are assigned to the binding energy of Cu $2p_{3/2}$ and Cu $2p_{1/2}$, respectively. The binding energy interval between Cu $2p_{3/2}$ and Cu $2p_{1/2}$ is about 20.2 eV, which represents the existence of copper as Cu^{2+} ions in the CuS network structure [23]. Much stronger Cu^{2+} satellite peaks located at 942.9 eV and 962.3 eV are observed in the Cu 2p spectrum of the sample, which further demonstrate the existence of Cu^{2+} [24]. It indicates that Cu will eventually be vulcanized into CuS after dealloying. Figure 4d represents the S 2p spectrum. The typical peak ranging from 160 eV to 164 eV is fitted by three peaks centering at 161.4 eV, 162.2 eV, and 163.2 eV, which corresponds to the binding energy of S-Cu [25–27]. A characteristic peak at 168.7 eV further proves the existence of metal sulfides [28]. Based on the analysis of the above XRD and XPS results, it can be concluded that CuS without any impurities is affirmed.
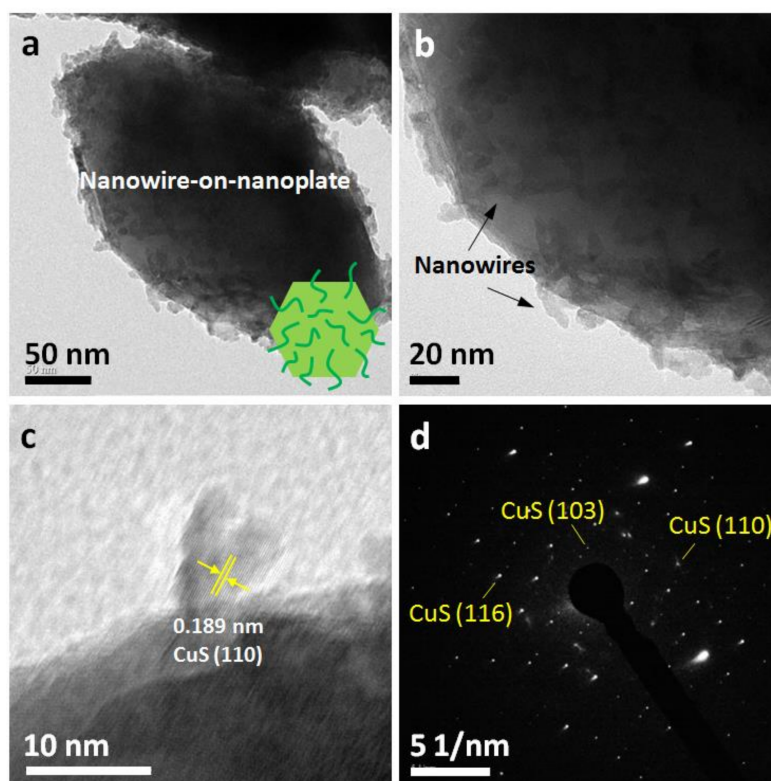
Figure 3. Transmission electron microscope (TEM) images (**a–c**) and corresponding selected area of the electron diffraction (SAED) pattern (**d**) of the as-obtained CuS.
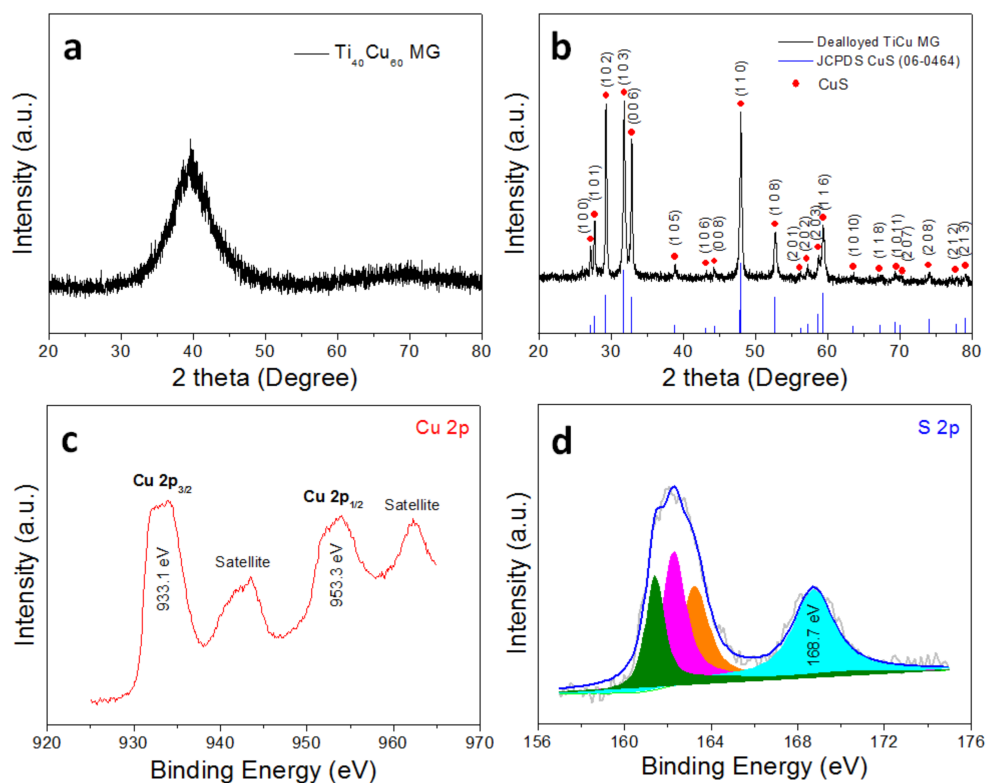

Figure 4. X-ray diffraction (XRD) patterns of the $Ti_{40}Cu_{60}$ ribbon before (**a**) and after dealloying (**b**). (**c,d**) X-ray photoelectron spectroscopy (XPS) spectrums of the as-obtained CuS: (**c**) Cu 2p, (**d**) S 2p.

It was reported that a reversible Li$^+$-intercalation/deintercalation process takes place at higher voltages (above approximately 1 V versus Li/Li$^+$) [29] through a number of intermediate phases with varying Li content. To continue the cycling series, CV and charge/discharge curves were tested in the potential range between 1 V to 3 V in this work. The CV curves of the CuS anode are shown in Figure 5a at a scanning rate of 0.1 mV·s^{-1} between 1.0 V to 3.0 V. During the first cathodic scan, two reduction peaks appear at 2.3 V and 1.52 V, which represents the transformation from CuS to Li$_x$CuS and the conversion of Li$_x$CuS to Cu, respectively [7]. In the subsequent scans, two reduction peaks shift to 2.06 V and 1.55 V. There is a clear difference in the peaks between the subsequent cycles and the first cycle, which can be attributed to the irreversible capacity loss and the formation of the solid electrolyte interface (SEI) film. In the anodic scan, two oxidation peaks can also be found at 1.94 V and 2.36 V, which is associated with the oxidation of Cu to CuS. The following equations [30,31] show the related electrochemical reactions.
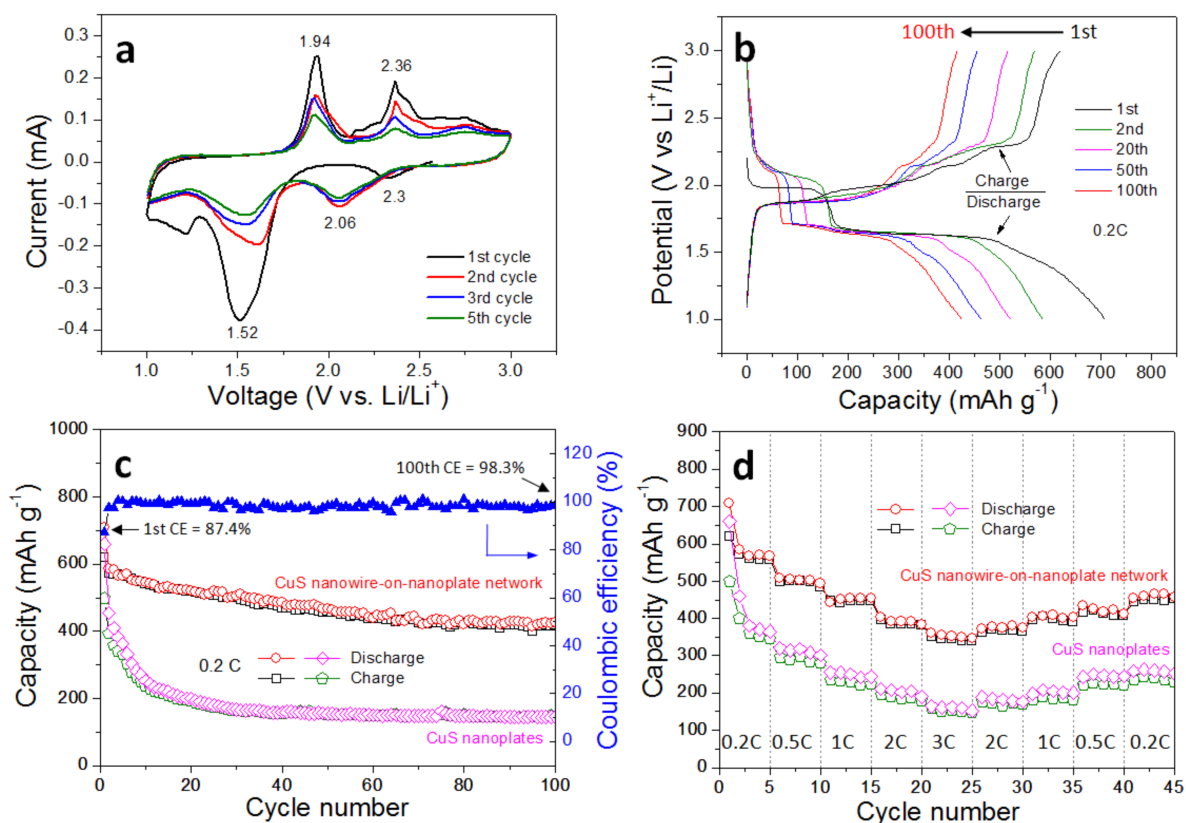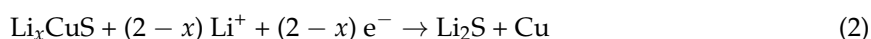
$$CuS + xLi^+ + xe^- \rightarrow Li_xCuS \tag{1}$$

$$Li_xCuS + (2 - x)\,Li^+ + (2 - x)\,e^- \rightarrow Li_2S + Cu \tag{2}$$

Figure 5. Electrochemical characterization of CuS anodes: (**a**) CV curves, (**b**) Charge/discharge curves at 0.2 C, (**c**) Cycling performance and coulombic efficiency, and (**d**) Rate capability.

Figure 5b shows the voltage-capacity curves of the CuS network electrode with different cycles at 0.2 C (1 C corresponds to 560 mA·g^{-1}). There are two potential plateaus to appear at 2.0 V to 2.2 V and 1.5 V to 1.7 V in its discharge process and two plateaus are located at around 1.8 V to 2.0 V and 2.2 V to 2.4 V in its charging cycle, which corresponds well with the CV data. The initial coulombic efficiency was 87.4%. The irreversible capacity loss can be attributed to the irreversible side reactions that occurred in the first discharge/charge process and the formation of the SEI film. From the 2nd to the 100th cycle, the discharge capacity gradually decreases from 585.4 mAh·g^{-1} to 425 mAh·g^{-1},

which indicates the continuous consumption of active materials and the sustaining formation of the SEI film.

Figure 5c presents both the cyclic performance and the coulombic efficiency data for the CuS electrodes. It can be seen that at 0.2 C, the CuS nanoplate electrode undergoes fast capacity decay. Its capacity is about 200.3 mAh·g^{-1} after the 20 cycles and only 145.3 mAh·g^{-1} after 100 cycles. By contrast, the CuS electrode with a nanowire-on-nanoplate network shows an improved cycling ability, which retains a capacity of 425 mAh·g^{-1} after 100 cycles. This is about 60% of the first discharge capacity (708 mAh·g^{-1}). Along with the satisfactory cycling performance, the CuS nanowire-on-nanoplate network exhibits an excellent coulombic efficiency of 98.3% even at the 100th cycle.

The rate capabilities of the CuS anodes are investigated in Figure 5d. The average capacities of the CuS nanoplate electrode are 391, 289.4, 228.2, and 187.6 mAh·g^{-1} at 0.2, 0.5, 1, and 2 C, respectively. When performed at 3 C, the average capacity drops to 152.2 mAh·g^{-1}. The capacity recovered to 236.7 mAh·g^{-1} when the rate returned to 0.2 C, which shows poor reversibility. On the other hand, when CuS nanowires were successfully generated into the CuS nanoplate network, it submits a reversible discharge capacity of about 560 mAh·g^{-1} at a low rate of 0.2 C. Furthermore, it delivers reversible discharge capacities of 502.6, 451.2, 392.3, and 352.4 mAh·g^{-1} at the rates of 0.5, 1, 2, and 3 C, respectively. When the rate reversed to 2, 1, 0.5, and 0.2 C, the capacity recovered to 375.9, 404.4, 422.5, and 460.5 mAh·g^{-1}, respectively, which indicated significantly promoted reversibility.

Figure 6 represents the electrochemical impendence spectroscopy (EIS) of the electrodes. The state of charge (SOC) of batteries in these tests is 100%. The high frequency semicircle in the Nyquist plot was connected with the charge transfer resistance of the electrode while the slope line at the low frequency is an indication of Warburg impedance of Li ions into active material diffusion. The curves indicate that there is some difference between two kinds of fresh CuS anodes in the electrical resistance. After 20 cycles, however, the charge-transfer resistance is reduced in the CuS nanowire-on-nanoplate network anode while it increased for the CuS nanoplate anode, which aligns with the cycling data.
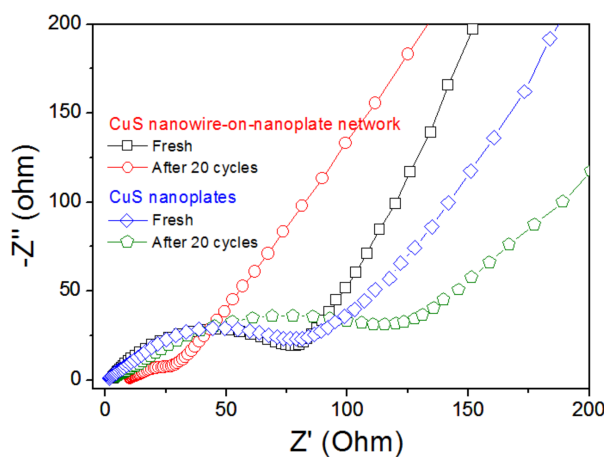

Figure 6. Nyquist plots of CuS electrodes.

As shown in Table 1 [6,7,31–35], the Li-ion storage performance of the as-obtained CuS nanowire-on-nanoplate network is superior to previous research studies. Compared to CuS nanospheres prepared by the microwave irradiation method [6], the expected final discharge capacity of the as-obtained CuS is about 395 mAh·g^{-1} at 0.36 C after 100 cycles, which indicates superior anode performance at a relatively high current density. The most valuable is the dealloying technique used in this study, which is a simple and low-cost route that reveals a fair balance between cost and performance. The performance enhancement in cycling and rate capability could be ascribed to the following three aspects. First, the introduction of CuS nanowires on the nanoplate network improves the specific surface area and offers a large number of active position for the Li-ion insertion/desertion.

Second, the nanowire-on-nanoplate network improves conductivity, reduces electrical resistance, and shortens the Li-ion diffusion length during cycling as compared to the bare CuS nanoplates structure. Third, the CuS nanowire-on-nanoplate network offers sufficient multiscale spaces including spaces among nanoplates, spaces among nanowires, and spaces between nanoplates and nanowires. These spaces are meant for volume expansion and shrinkage, which is conducive to remitting the capacity attenuation during repeating charge/discharge cycles.

Table 1. Comparative performance of CuS anodes for LIBs applications.

Anode Material	Preparation Method	Current Density	Cycle Number	Final Discharge Capacity (mAh·g^{-1})	Reference
Hierarchical CuS/graphene	Hydrothermal method	0.09 C	100	568	[7]
CuS-rGO	Hydrothermal process	0.18 C	50	451	[31]
CuS/graphene composite	Hydrothermal method	0.09 C	25	296	[32]
CuS nanospheres	Microwave irradiation method	0.36 C	100	379	[6]
CuS particles	Hydrothermal process	0.2 C	100	159.7	[33]
CuS coated on Cu foil	Spray pyrolysis	0.1 C	30	450	[34]
CuS nanosheet network	In situ melt-diffusion strategy	0.2 C	100	468.3	[35]
CuS nanowire-on-nanoplate network	Dealloying	0.2 C	100	425 (395/expected at 0.36 C)	This work

4. Conclusions

In summary, the CuS nanowire-on-nanoplate network was synthesized by an improved dealloying route under two contrasting reaction temperatures. It showed that CuS nanoplates with a big size were synthesized under a reletively high temperature. CuS nanowires were subsequently prepared on the nanoplates under a reletively low temperature. The new strategy opens a door for us to design and fabricate dealloying products in various shapes and create more interesting composite structures. The electrochemical performances of the materials as anodes for LIBs were measured. The first discharge capacity of the CuS electrode reached 708 mAh·g^{-1} at 0.2 C and it remained at 425 mAh·g^{-1} during the 100th cycle. However, it still exhibited a stable capacity around 350 mAh·g^{-1} at 3 C. The results prove that the design strategy for improving the connectivity and conductivity of anode materials is beneficial. The as-designed nanowire-on-nanoplate network structure including the multiscale spaces improved connectivity, conductivity, specific surface area, and Li storage sites, which guarantees adequate cycling and rate performance. This paper not only develops the dealloying technique but also shows an effective structural design to acquire advanced anode materials with satisfactory connectivity for LIBs.

Author Contributions: Zhifeng Wang, Yongguang Zhang, and Chunling Qin conceived and designed the experiments. Xiaomin Zhang and Man Li performed the experiments. Zhumabay Bakenov and Chunling Qin contributed reagents, materials, and analysis tools. Zhifeng Wang and Yongguang Zhang wrote the paper.

Conflicts of Interest: The authors declare no conflict of interest.

References

1. Kennedy, T.; Brandon, M.; Ryan, K.M. Advances in the application of silicon and germanium nanowires for high-performance lithium-ion batteries. *Adv. Mater.* **2016**, *28*, 5696–5704. [CrossRef] [PubMed]
2. Zhang, Y.G.; Li, Y.; Li, H.P.; Yin, F.X.; Zhao, Y.; Bakenov, Z. Synthesis of hierarchical MoS$_2$ microspheres composed of nanosheets assembled via facile hydrothermal method as anode material for lithium-ion batteries. *J. Nanopart. Res.* **2016**, *63*, 1–9. [CrossRef]

3.   McNulty, D.; Geaney, H.; Buckley, D.; O'Dwyer, C. High capacity binder-free nanocrystalline GeO$_2$ inverse opal anodes for Li-ion batteries with long cycle life and stable cell voltage. *Nano Energy* **2018**, *43*, 11–21. [CrossRef]

4.   Zhang, Y.G.; Li, Y.; Li, H.P.; Yin, F.X.; Bakenov, Z. Electrochemical performance of carbon-encapsulated Fe$_3$O$_4$ nanoparticles in lithium-ion batteries: Morphology and particle size effects. *Electrochim. Acta* **2016**, *216*, 475–483. [CrossRef]

5.   Wang, Y.H.; Zhang, Y.Y.; Li, H.; Peng, Y.Y.; Li, J.Y.; Wang, J.; Hwang, B.J.; Zhao, J.B. Realizing high reversible capacity: 3D intertwined CNTs inherently conductive network for CuS as an anode for lithium ion batteries. *Chem. Eng. J.* **2018**, *332*, 49–56. [CrossRef]

6.   Li, H.; Wang, Y.H.; Huang, J.X.; Zhang, Y.Y.; Zhao, J.B. Microwave-assisted synthesis of CuS/graphene composite for enhanced lithium storage properties. *Electrochim. Acta* **2017**, *225*, 443–451. [CrossRef]

7.   Ding, C.H.; Su, D.Z.; Ma, W.X.; Zhao, Y.J.; Yan, D.; Li, J.B.; Jin, H.B. Design of hierarchical CuS/graphene architectures with enhanced lithium storage capability. *Appl. Surf. Sci.* **2017**, *403*, 1–8. [CrossRef]

8.   Li, H.; Wang, Y.H.; Jiang, J.L.; Zhang, Y.Y.; Peng, Y.Y.; Zhao, J.B. CuS microspheres as high-performance anode material for Na-ion batteries. *Electrochim. Acta* **2017**, *247*, 851–859. [CrossRef]

9.   Chen, H.; Yeh, Y.M.; Chen, Y.T.; Jiang, Y.L. Influence of growth conditions on hair-like CuS nanowires fabricated by electro-deposition and sulfurization. *Ceram. Int.* **2014**, *40*, 9757–9761. [CrossRef]

10.   Zhou, M.J.; Peng, N.; Liu, Z.; Xi, Y.; He, H.Q.; Xia, Y.G.; Liu, Z.P.; Okada, S. Synthesis of sub-10 nm copper sulphide rods as high-performance anode for long-cycle life Li-ion batteries. *J. Power Sources* **2016**, *306*, 408–412. [CrossRef]

11.   Du, Y.P.; Yin, Z.Y.; Zhu, J.X.; Huang, X.; Wu, X.J.; Zeng, Z.Y.; Yan, Q.Y.; Zhang, H. A general method for the large-scale synthesis of uniform ultrathin metal sulphide nanocrystals. *Nat. Commun.* **2012**, *3*, 1177. [CrossRef] [PubMed]

12.   Zhao, L.; Tao, F.Q.; Quan, Z.; Zhou, X.L.; Yuan, Y.H.; Hu, J.C. Bubble template synthesis of copper sulfide hollow spheres and their applications in lithium ion battery. *Mater. Lett.* **2012**, *68*, 28–31. [CrossRef]

13.   Sabah, F.A.; Ahmedad, N.M.; Hassan, Z.; Almessiere, M.A. A novel CuS thin film deposition method by laser-assisted spray photolysis deposition and its application to EGFET. *Sens. Actuators B Chem.* **2017**, *247*, 197–215. [CrossRef]

14.   Hu, X.S.; Shen, Y.; Xu, L.H.; Wang, L.M.; Xing, Y.J. Preparation of flower-like CuS by solvothermal method and its photodegradation and UV protection. *J. Alloys Compd.* **2016**, *674*, 289–294. [CrossRef]

15.   Lu, Z.; Li, C.; Han, J.H.; Zhang, F.; Liu, P.; Wang, H.; Wang, Z.L.; Cheng, C.; Chen, L.H.; Hirata, A.; Fujita, T.; Erlebacher, J.; Chen, M.W. Three-dimensional bicontinuous nanoporous materials by vapor phase dealloying. *Nat. Commun.* **2018**, *9*, 276. [CrossRef] [PubMed]

16.   Fujita, T.; Higuchi, K.; Yamamoto, Y.; Tokunaga, T.; Arai, S.; Abe, H. In-situ TEM study of a nanoporous Ni–Co catalyst used for the dry reforming of methane. *Metals* **2017**, *7*, 406. [CrossRef]

17.   Xu, C.X.; Wang, R.Y.; Zhang, Y.; Ding, Y. A general corrosion route to nanostructured metal oxides. *Nanoscale* **2010**, *2*, 906–909. [CrossRef] [PubMed]

18.   Wang, Z.F.; Fei, P.Y.; Xiong, H.Q.; Qin, C.L.; Zhao, W.M.; Liu, X.Z. CoFe$_2$O$_4$ nanoplates synthesized by dealloying method as high performance Li-ion battery anodes. *Electrochim. Acta* **2017**, *252*, 295–305. [CrossRef]

19.   Xu, W.C.; Liang, Y.Q.; Su, Y.G.; Zhu, S.L.; Cui, Z.D.; Yang, X.J.; Inoue, A.; Wei, Q.; Liang, C.Y. Synthesis and properties of morphology controllable copper sulphide nanosheets for supercapacitor application. *Electrochim. Acta* **2016**, *211*, 891–899. [CrossRef]

20.   Xu, W.C.; Zhu, S.L.; Liang, Y.Q.; Li, Z.Y.; Cui, Z.D.; Yang, X.J.; Inoue, A. Nanoporous CuS with excellent photocatalytic property. *Sci. Rep.* **2015**, *5*, 15125. [CrossRef] [PubMed]

21.   Wang, Z.F.; Liu, J.Y.; Qin, C.L.; Liu, L.; Zhao, W.M.; Inoue, A. Fabrication and new electrochemical properties of nanoporous Cu by dealloying amorphous Cu–Hf–Al alloys. *Intermetallics* **2015**, *56*, 48–55. [CrossRef]

22.   Zhao, W.M.; Fei, P.Y.; Zhang, X.M.; Zhang, Y.G.; Qin, C.L.; Wang, Z.F. Porous TiO$_2$/Fe$_2$O$_3$ nanoplate composites prepared by de-alloying method for Li-ion batteries. *Mater. Lett.* **2018**, *211*, 254–257. [CrossRef]

23.   Venkadesh, A.; Radhakrishnan, S.; Mathiyarasu, J. Eco-friendly synthesis and morphology-dependent superior electrocatalytic properties of CuS nanostructures. *Electrochim. Acta* **2017**, *246*, 544–552. [CrossRef]

24. Qin, C.L.; Zhang, Y.S.; Wang, Z.F.; Xiong, H.Q.; Yu, H.; Zhao, W.M. One-step synthesis of CuO@brass foil by dealloying method for low-cost flexible supercapacitor electrodes. *J. Mater. Sci. Mater. Electron.* **2016**, *27*, 9206–9215. [CrossRef]

25. Karikalan, N.; Karthik, R.; Chen, S.M.; Karuppiah, C.; Elangovan, A. Sonochemical synthesis of sulfur doped reduced graphene oxide supported CuS nanoparticles for the non-enzymatic glucose sensor applications. *Sci. Rep.* **2017**, *7*, 2494. [CrossRef] [PubMed]

26. Gao, L.G.; Du, J.W.; Ma, T.L. Cysteine-assisted synthesis of CuS-TiO$_2$ composites with enhanced photocatalytic activity. *Ceram. Int.* **2017**, *43*, 9559–9563. [CrossRef]

27. Hu, X.S.; Shen, Y.; Zhang, Y.T.; Zhang, H.F.; Xu, L.H.; Xing, Y.J. Synthesis of flower-like CuS/reduced graphene oxide (RGO) composites with significantly enhanced photocatalytic performance. *J. Alloys Compd.* **2017**, *695*, 1778–1785. [CrossRef]

28. Song, C.D.; Wang, X.; Zhang, J.; Chen, X.B.; Li, C. Enhanced performance of direct Z-scheme CuS-WO$_3$ system towards photocatalytic decomposition of organic pollutants under visible light. *Appl. Surf. Sci.* **2017**, *425*, 788–795. [CrossRef]

29. Hosseinpour, Z.; Scarpellini, A.; Najafishirtari, S.; Marras, S.; Colombo, M.; Alemi, A.; De Volder, M.; George, C.; Lesnyak, V. Morphology-dependent electrochemical properties of CuS hierarchical superstructures. *ChemPhysChem* **2015**, *16*, 3418–3424. [CrossRef] [PubMed]

30. Tang, J.; Ni, S.B.; Chen, Q.C.; Zhang, J.C.; Yang, X.L. CuS@Cu freestanding electrode via electrochemical corrosion for high performance Li-ion batteries. *Mater. Lett.* **2017**, *201*, 13–17. [CrossRef]

31. Wang, J.X.; Lyu, X.J.; Wang, L.Y.; Yu, S.; Zhu, W.X.; Han, C.; Cao, X.Q. Preparation and electrochemical performance of hierarchical CuS-rGO composite. *J. Alloys Compd.* **2017**, *694*, 1067–1072. [CrossRef]

32. Tao, H.C.; Yang, X.L.; Zhang, L.L.; Ni, S.B. One-pot facile synthesis of CuS/graphene composite as anode materials for lithium ion batteries. *J. Phys. Chem. Solids* **2014**, *75*, 1205–1209. [CrossRef]

33. Ren, Y.R.; Wei, H.M.; Yang, B.; Wang, J.W.; Ding, J.N. "Double-sandwich-like" CuS@reduced graphene oxide as an anode in lithium ion batteries with enhanced electrochemical performance. *Electrochim. Acta* **2014**, *145*, 193–200. [CrossRef]

34. Kalimuldina, G.; Taniguchi, I. Electrochemical properties of stoichiometric CuS coated on carbon fiber paper and Cu foil current collectors as cathode material for lithium batteries. *J. Mater. Chem. A* **2017**, *5*, 6937–6946. [CrossRef]

35. Cheng, J.J.; Pan, Y.; Zhu, J.T.; Li, Z.Z.; Pan, J.N.; Ma, Z.S. Hybrid network CuS monolith cathode materials synthesized via facile in situ melt-diffusion for Li-ion batteries. *J. Power Sources* **2014**, *257*, 192–197. [CrossRef]